13B.4 CPOL RADAR-DERIVED DSD STATISTICS OF STRATIFORM AND CONVECTIVE RAIN FOR TWO REGIMES IN DARWIN, AUSTRALIA

M. Thurai[1*], V. N. Bringi[1], and P. T. May[2]

[1]Colorado State University, Fort Collins, Colorado, USA
[2]Centre for Australian Weather and Climate Research, Australia

1. INTRODUCTION

In a recent publication, Bringi et al. (2009) describe the retrieval of drop size distribution (DSD) parameters and rain rate from the C-band polarimetric radar (i.e., the CPOL radar, as described by Keenan et al. 1998) located near Darwin, Australia. The normalized gamma DSD (Testud et al. 2001) was used, described by the parameters D_0 representing the median volume diameter (D_0) and N_W rerpesenting the 'generalized' intercept parameter. The N_W is the same as the intercept parameter (N_0) of an exponential DSD that has the same D_0 and water content as the gamma DSD.

In the aforementioned work of Bringi et al. (2009), a simple DSD-based indexing scheme was introduced which enabled the convective and stratiform rain to be separated as well as the 'mixed' or 'uncertain' rain regions to be identified from the CPOL scans (after the copolar and differential attenuation corrections). The indexing scheme was primarily developed from dual-frequnecy profiler observations, from which the normalized gamma DSD parameters were retrieved using the technique described in Williams and Gage (2009). Easy identification of rain type was made possible based on the vertical profiles of reflectivity and mean Doppler velocity (vertical). The DSD-based classification was then applied to polarimetric radar-based retrievals and the initial application of the indexing scheme was shown to be useful not only in the classification of rain types from CPOL data but also to derive the pdf (probability density function) of D_0 and $\log_{10}(N_W)$, separately for convective and stratiform rain types.

There is a large body of literature that deals with classification of stratiform and convective rain types (mainly in the tropics) based on different methods such as the use of reflectivity texture (e.g., Steiner et al. 1995), magnitude of up/down drafts (e.g., Atlas et al. 2000), surface disdrometer measurements (e.g., Tokay and Short 1996) and profiler data (Williams et al. 1995). More recently, Ulbrich and Atlas (2007) show that it is important to identify the transition rain type whose DSD characteristics are sufficiently different from the purely convective and stratiform DSDs with the result that three different Z-R relations are needed to accurately estimate the rainfall. They also show that the convective DSDs in the tropics frequently fall into the equilibrium-like form when the transition rain is separated from the purely convective rain. The transition rain type is somewhat similar to the 'mixed convective/stratiform' class introduced by Williams et al. (1995).

In this paper, we present more details of the DSD-based indexing technique and compare the results of our classification with some of the previously published work. Later, in section 4, we present statistics of the DSD parameters for two 'seasons' in Darwin, namely build-up (or premonsoon) and monsoon. The results are given in terms of pdf and conditional pdf (i.e. conditioned to Z intervals).

*Corresponding author address: Merhala Thurai, Dept. of Electrical Engineering, Colorado State University, Fort Collins, CO 80523-1373, USA.
Email: merhala@engr.colostate.edu

2. BASIS FOR THE SEPARATION TECHNIQUE

2.1 Previous study in Darwin

In the earlier study by Bringi et al., (2009) involving DSD retrievals from the combination of CPOL radar and dual-frequency profiler observations, it was noted that the convective and stratiform rain could be separated by utilizing the variation between the two main parameters defining the DSD, *viz.* N_W and D_0. The study initially examined the vertical profiles of the DSDs retrieved and extracted from CPOL RHI scans taken over the dual-frequency profiler site, the data being taken during the TWP-ICE campaign (May et al. 2008). The retrieval of DSDs from the CPOL radar data, as well as the comparison with those retrieved from the dual-frequency profiler (50 MHz and 920 MHz) are fully explained in the earlier study (Bringi et al., 2009) and hence will not be repeated here. However, we summarize here the outcome of our observations relating to the CPOL-retrieved DSDs and the simultaneous observations from the dual-frequency profiler.

Initially, an event consisting of intense convection, followed by stratiform rain with a clear 'bright-band' was analyzed. Regions of strong updraft from the 50 MHz profiler observations occurring for the first half hour of the event were seen to be associated with

reflectivity profiles consistent with strong convection from the 920 MHz profiler observations as well as CPOL data over the profiler site, where 30 dBZ reflectivity values were observed at altitudes extending to nearly 13 km. By contrast, a later period (from ~ one hour after the start of the event) showed stratiform rain with 'bright-band' being clearly visible in the 4.5 – 5 km altitude, this rain type lasting two further hours and being associated with low or near-zero vertical Doppler velocities from the 50 MHz profiler.

When the DSD characteristics retrieved from the dual-frequency profiler data for this event were analyzed, it showed a clear separation in terms of the N_W versus D_0 variation. There were three regions: (i) the retrievals during the convective part of the event; (ii) those during longer duration stratiform rain and (iii) the transition rain (Ulbrich and Atlas 2007) for the period in-between (i) and (ii). A 'separator line' was drawn after visual inspection of a number of datasets, given by the equation

$$\log_{10}\left(N_w{}^{sep}\right) = c_1 D_0 + c_2 \qquad (1)$$

where c_1 lies in the region -1.6 to -1.7 and c_2 lies in the region 6.3 to 6.4. In (1), D_0 is in units of mm and N_W in $mm^{-1}\ m^{-3}$.

The separation of the stratiform and convective rain types was clearly observed and moreover, the transition region was seen to 'straddle' the straight line of (1). An index term '*i* ' was then defined as follows:

$$i = \log_{10}\left(N_w{}^{est}\right) - \log_{10}\left(N_w{}^{sep}\right) \qquad (2)$$

where $N_W{}^{est}$ represents the estimated N_W from the direct measurements (profiler or radar) and $N_W{}^{sep}$ represents the output of (1) when D_0 is set to the estimated D_0 value from the (profiler or radar) measurements.

Variation of the value of `i´ with vertical wind velocity, determined from the dual-frequency profiler data is shown in Fig. 1 for the abovementioned event. Only the heights in the 1.5 to 2.7 km range were considered in order to ensure that the variation is confined to the rain region. Clearly visible from Fig. 1 is the stark contrast between the negative values of i which correspond to low wind velocity and the positive values of i, which correspond to high vertical wind velocity, which in turn are associated with stratiform rain and convective rain respectively.

Moreover, values of i determined from the CPOL measurements extracted from RHI scans over the profiler site showed stratiform rain type being indicated by significant negative values of i < -0.1 and convective rain type being indicated by significant positive values of i > 0.1 (see section 4.1 of Bringi et al. 2009). For the in between values of i (i.e. magnitude of i ≤ 0.1), the region corresponded to what we term here as the 'mixed' or 'uncertain' type (and not necessarily as transition rain as defined by Ulbrich and Atlas 2007). Henceforth we use the term 'mixed' type when magnitude i < 0.1.

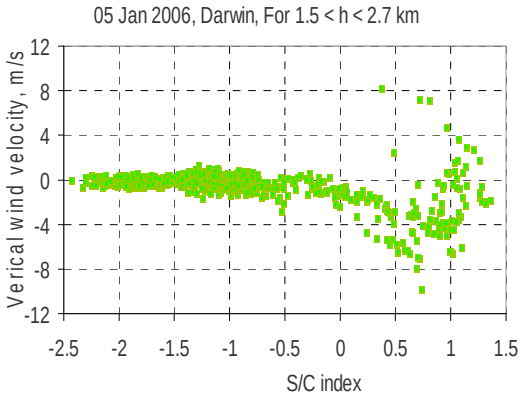

Fig. 1: Variation of the value of ´i` with vertical wind velocity from the dual frequency measurements for the 05 Jan 2006 event. Negative values of i correspond to low vertical wind velocity (associated with stratiform rain) and the positive values of i correspond to larger velocities (associated with convection).

Based on the above observations, it was concluded that the value of the index *i* determined from the CPOL measurements can be used as an indicator of the likelihood of the rain-type as being stratiform, convective or 'mixed'. The indexing technique was also applied to an example PPI which clearly showed regions of embedded convection during a widespread event.

2.2 Global DSD characteristics

Bringi et al. (2003) have examined the variability of the DSD characteristics across different climatic regions in terms of $\log_{10}(N_W)$ versus D_m (the mass-weighted mean diameter) for stratiform and convective rain separately. An unmarked version of their data points is given in Fig. 2. The variations were determined using disdrometer measurements (the 2D-video disdrometer or Joss-Waldvogel types) as well as from polarimetric radar data for stratiform (blue) and convective rain (red). The disdrometer data used in these calculations represent 2-minute averaged DSDs and a simple classification of stratiform rain was based on the standard deviation of rainfall rate R over 5 consecutive samples being < 1.5 mm/h. For the radar data, stratiform rain was classified using bright–band identification.

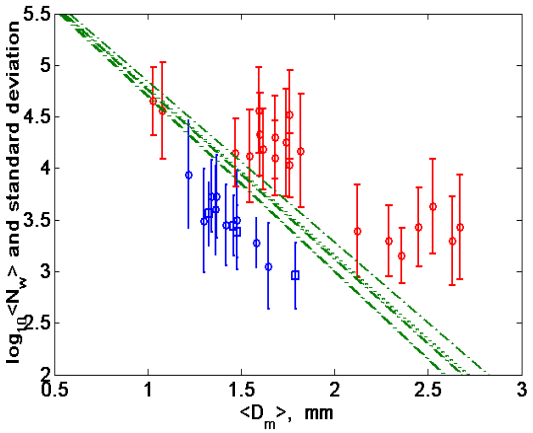

Fig. 2: The average value of $\log_{10}(N_W)$ with ± 1σ (standard deviation) bars versus average D_m from disdrometer (open circles) and dual-polarization radar (open squares) for various locations given in Bringi et al. (2003) for stratiform rain (in blue) and convective rain (red). The data are from different locations. The green lines represent our equation (1) determined independently from the Darwin observations, with D0 converted to Dm using μ values of -2, 0, 3 and 5.

In Fig. 1(a) and (b), we include our separator line from (1), assuming a specific value for the shape parameter μ as shown in the figure caption. In all but two data points with low D_m (~ 1 mm), the stratiform rain events lie below and the convective events lie above the separator line. The two data points which lie 'on' our separator line (with D_m of around 1 mm) were determined for warm shallow rain in Okinawa using the C-band polarimetric radar, COBRA, where there were difficulties in clear separation of the rain types. These two cases would perhaps qualify as being 'mixed' or 'uncertain'.

The overall implication of Fig. 2 is that our equation (1) may be applicable to several other locations, which enables the stratiform/convective rain classification to be automatically performed on a pixel by pixel basis from polarimateric radar PPI scans.

3. TESTING OF THE METHODOLOGY

3.1 Monsoon regime case

Here we compare the DSD-based technique with the Steiner et al. (1995) texture-based algorithm (henceforth referred to as SHY). The latter uses the intensity and sharpness of the peaks of radar reflectivity relative to the 'background' reflectivity, with the peaks indicating the centers of the convective regions. They used the C-band TOGA (Tropical Ocean Global Atmosphere) radar located in Darwin to fine-tune their convective rain classification using gridded data for the month of February 1988. In their scheme, all areas which are not classified as convective were automatically assigned as stratiform. To compare our DSD-based index classification with the SHY scheme we have chosen one volume scan from 22 January 2006 which is representative of the monsoon regime.

Fig. 3a shows the attenuation-corrected reflectivity data from CPOL radar measurements as a CAPPI (constant altitude PPI) at 2.5 km altitude. This event was deemed suitable for our testing since it was a wide spread event with intense convective squall line, large stratiform areas with embedded convection, and extending over both land and ocean. The SHY scheme was applied to this data as well as our DSD-based indexing scheme (which as mentioned before gives three classification of rain types, i.e., convective, stratiform and 'mixed'). Figs. 3b and 3c show the rain type classification using our method and the SHY method, respectively. In both cases, the light blue represents stratiform rain type and the red areas represent convective rain. The green areas in Fig. 3b represent the regions classified as being 'mixed'. The output of the two classification schemes is over-plotted in Fig. 3d, where the SHY output is represented by black contours for convective areas.

Overall, there seems good agreement between the two classification methods except for small areas (within larger SHY classified convective areas) near (x,y; km) at (-140,-10), (-20,-100) and (110, 80). However, in general, the convective classification areas from the SHY method seem to encompass the convective and 'mixed' areas from the indexing scheme. The regions classified as being stratiform rain agree well between the SHY method and the indexing scheme.

To quantify the 'mis-classification' by the SHY method, out of a total of 8453 pixels where the attenuation-corrected Z_h was greater than 10 dBZ, there were only 60 pixels where the SHY method classified rain type as being stratiform whilst our indexing scheme did not, and only 210 pixels where the SHY method classified as being convective whilst our indexing scheme did not. Even if we assume - for the sake of argument that the SHY method is 'correct', the number of cases with disagreement when compared with our indexing scheme is only about 3.2% of the total. This percentage further reduces to 1.0 % if the radar range is restricted to 90 km, which is clearly very small when considering the totally different methodologies used.

3.2 Statistics of the rain DSD

Statistical comparisons of the polarimetrically-derived DSD parameters within the different rain types were also performed utilizing all CAPPIs at 2.5 km altitude for the Monsoon period (13 to 23 January 2006).

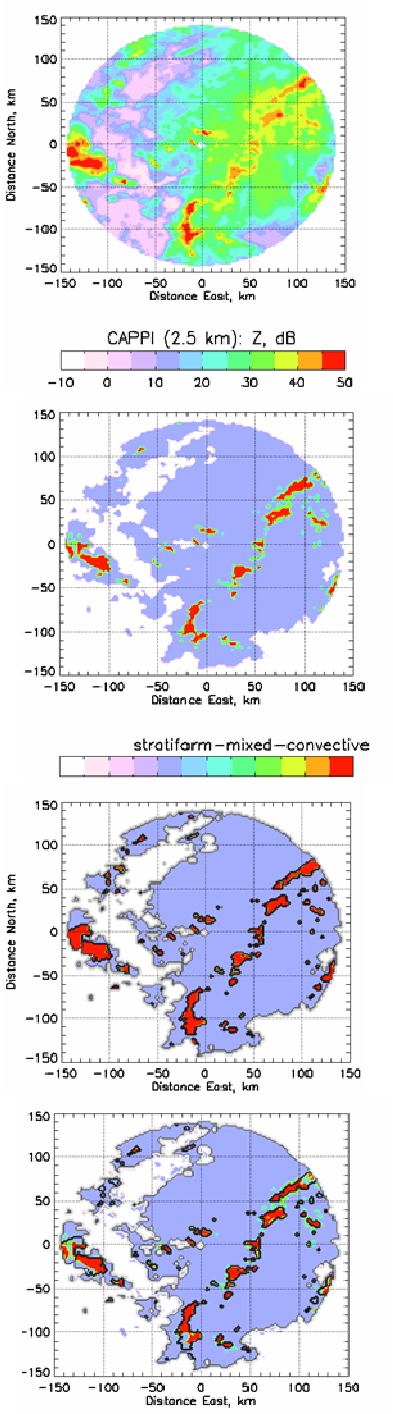

Fig. 3: (a) Constructed CAPPI reflectivity data from CPOL volume scans taken on 22 Jan 2006 (at around 15:00 UTC), (b) rain type classification using the indexing scheme, (c) rain type classification using the SHY method, and (d) the indexing scheme (in color) with the SHY method over-plotted as black contours for convective rain type.

Results are shown in the 4 panels in Fig. 4 in terms of relative frequency histograms of D_0 and $\log_{10}(N_W)$ for stratiform and convective rain types. The results from the SHY texture method is shown in pink whilst our index-based method is shown in dark blue. To clarify, the D_0 and $\log_{10}(N_W)$ values from the SHY texture method only means that the DSD-parameters we derived were from pixels classified by the SHY method as being either stratiform or convective. It should be clear that the SHY method contains no information on the DSD parameters.

Because of the large number of points (~10s of thousands) used to construct the histograms, one may assume that the histograms would have 'converged' to the underlying pdf.

The following points can be made from Fig. 4:

- for rain type classified as stratiform (top panels), there is hardly any difference in the statistics (e.g., mode, width and skewness), both for D_0 and for log10(N_W);
- for convective rain type, the histogram for D_0 is again in excellent agreement; however, the SHY texture method gives rise to a small percentage of cases with D_0 values less than 0.8 mm;
- additionally for convective rain, the texture method gives a 'long tail' at the lower end of the log10(N_W) histogram whereas the index-based method is more symmetric and does not show any cases with $\log_{10}(N_W) < 3.2$, which is more realistic (and in agreement with Testud et al. 2001; their Figs. 5 and 6). The 'long tail' in $\log_{10}(N_W)$ for convective rain is perhaps due to misclassification of the texture method and should have been classified as stratiform rain type.

3.3 N_0 – R based classification

Our final comparison entails the use of N_0 - R (Tokay and Short 1996; henceforth TS) separator line to classify between stratiform and convective rain types. TS used Joss disdrometer (Joss and Waldvogel 1967) data from the TOGA-COARE (Coupled Ocean Atmosphere Response Experiment) and their database represents tropical oceanic storms. TS found that stratiform and convective rain types, from their database, occupied two distinct domains separated by an N_0 - R relation:

$$N_0 = 4.0 * 10^9 R^{-4.3} \qquad (3)$$

Fig. 5 shows the separator (dashed line) equivalent to (3) in the N_0 – R domain as a solid black line. Also shown is the scatter plot of $\log_{10}(N_0)$ versus R values

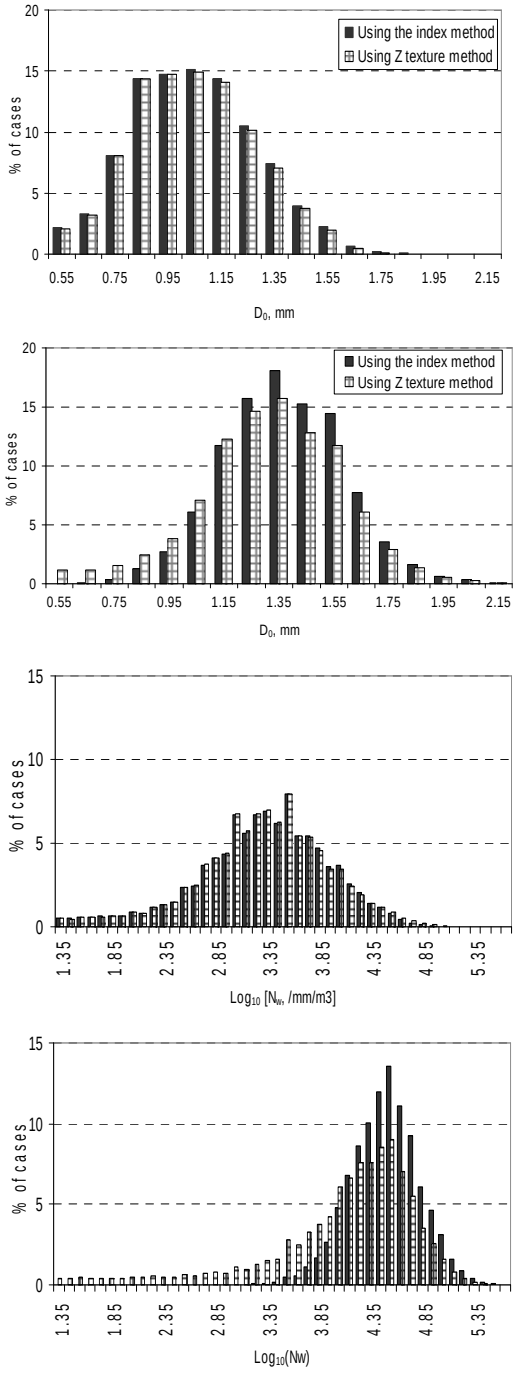

Fig. 4: Histogram comparisons (in terms of percentage probability) between the indexing technique and the SHY method; (a) D_0 for stratiform rain, (b) D_0 for convective rain, (c) N_W for stratiform rain, and (d) N_W for convective rain. The bin centers have been slightly displaced for clarity.

from the 22 January 2006 CAPPI data described earlier in Section 3a. Note that N_0 is the un-normalized scaling parameter of the gamma DSD form used by Ulbrich (1983) whereas N_W is the intercept parameter of an equivalent exponential DSD that has the same D_0 and water content as the normalized gamma DSD (Testud et al. 2001). Since our polarimetric radar algorithm estimates N_W, we convert to N_0 assuming the shape parameter μ=1 and equation (7.63) from Bringi and Chandrasekar (2001). The rain rate R is based on a 'synthetic' algorithm that uses (Z_h, Z_{dr} and K_{dp}) as described in Bringi et al. (2009).

In Fig. 5, the blue points represent stratiform rain, the red points represent convective rain and the green points the 'mixed' type. The TS line does separate the stratiform and convective points very well; however, our 'mixed' points fall on the convective 'side' of the separator line. Atlas et al. (1999) point out that the convective Z-R relation of TS actually represents a mix of convective and transition DSDs which is in general agreement with Fig. 4. Higher values of μ were also attempted (such as 3 and 5, not shown here) but μ = 1 seems to be reasonable. While large values of μ (3-12) have been inferred by Atlas et al. (1999) for the TOGA-COARE data set using Joss disdrometer data, we find that such values, if used to convert from N_W to N_0, would result in very poor ability of TS's N_0 - R separator line to be applicable to test our classification. We note that contrary to the large μ values (5-12) obtained by Atlas et al. (1999) and Ulbrich and Atlas (2007), the normalized gamma fits to airborne imaging probe DSD data from TOGA-COARE by Testud et al (2001) show average μ for stratiform rain to be 0.78 whereas for convective rain (< 30 mm h-1) it was in the range 1.51-1.78. Hence, our choice of μ = 1 is not unreasonable for converting N_W to N_0 in order to compare our classification to that of TS.

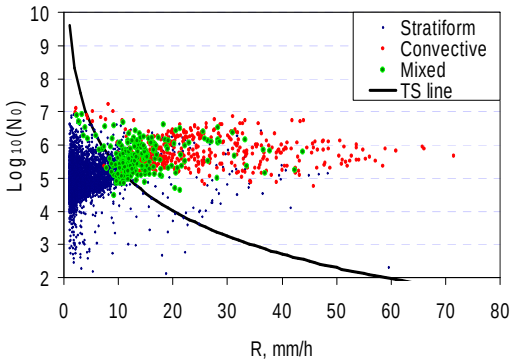

Fig. 5: $Log_{10}(N_0)$ versus rainfall rate for stratiform, convective and 'mixed' rain types for the CAPPI in Fig 1(a) using the indexing scheme output in Fig. 1(b) and assuming μ=1. The black line represents the Tokay and Short (1996) separation line, given by (3).

Several caveats are in order here. First, the TS's N_0 - R separator line was based on tropical storms occurring over the open ocean while our data is from Darwin (coastal location) and includes data from land and ocean (see CAPPI in Fig. 1). Second, our classification is based on radar data with large resolution volumes as compared with surface disdrometers. Considering these two factors, our classification results are in good agreement with TS's N_0 - R separator line and sufficient to serve as a sanity check on our indexing scheme.

Finally we note from Fig. 4 that using a simple R=10 mm h^{-1} threshold is, in fact, reasonable for delimiting stratiform (blue dots) from convective rain types (red dots). Such a threshold was used by Testud et al. (2001) for classification using rain rate data derived from an airborne particle probe from flights during TOGA COARE. They simply considered…" an along-track series $\{R_i\}$…if R_k and 10 adjacent values (from R_{k-5} to R_{k+5}) are all less than 10 mm h^{-1}, then spectrum k is considered to be stratiform rain; otherwise, spectrum k is classified as convective". Their simple approach lends further credence to our indexing scheme and more importantly to our 'synthetic' rain rate algorithm described in Bringi et al. (2009).

4. HISTOGRAMS OF D_0 AND N_W

Our index-based scheme was applied to all of the CPOL data taken during the pre-Monsoon (or build-up) period and the active Monsoon period during the TWP-ICE (Tropical Warm Pool-International Cloud Experiment). According to May et al. (2008), the active Monsoon period in 2006 was from 13 to 23 January. For the pre-Monsoon period (also called the build-up period), the data were taken from 01 November to 30 December 2005.

Our data processing was performed using PPI data and the DSD parameters (N_W, D_0) and R were retrieved for all 1.1° elevation PPI sweeps up to a range of 80 km (see Bringi et al. 2009 for details). Our indexing method was then applied to automate the rain-type classification in order to obtain D_0 and N_W histograms for convective, stratiform and 'mixed' rain types. The histograms were further separated into over-land and over-ocean regions, with the following range and azimuth limits (see also Fig. 6)

Land: 115-215° azimuth and 10-80 km range; (area ~ 5500 km^2)

Ocean: 240-285° azimuth and 10-80 km range; (area ~ 2500 km^2)

Relative frequency histograms (in essence, the pdf) of D_0 are shown in Fig. 7 for build-up and Monsoon regimes, for stratiform and convective rain types, and for over-land and ocean areas. Convective rain shows differences in D_0 histograms between the build-up and the Monsoon, with the former having higher D_0 values, both over land and over ocean. This is not surprising given that the build-up regime would have stronger updrafts and higher average vertical reflectivity profiles extending above the 0 deg C isotherm relative to the Monsoon regime. For stratiform rain, the differences across the two regimes are relatively small, particularly over ocean.

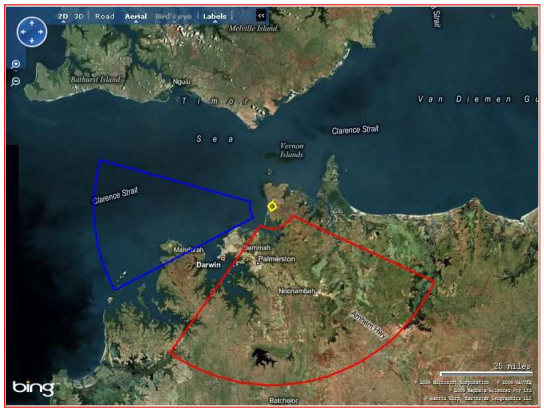

Fig. 6: Location of CPOL radar near Darwin marked as yellow diamond. The red polar 'box' delineates the land area while the blue polar 'box' denotes the ocean area.

Table 1 shows the mean, the standard deviation and skewness parameters, as well as the percentage and number of pixels of occurrence for stratiform, convective and 'mixed' rain types. In all cases, stratiform rain is, as expected, seen to dominate, with percentage of occurrence in the range 87-89%, while for convective rain it is 7.7-9%, and for 'mixed' it is 2.5-3%. These values are fairly consistent with SHY results for February 1988 season in the Darwin area of 88% stratiform and 12% convective, if in our case we lump the convective and 'mixed' into the convective category. Several points may be noted from Table 1:

- The largest differences are in convective rain between build-up and Monsoon regimes (independent of land or ocean areas).
- Stratiform rain histograms are very similar across regimes and land-ocean areas with slight deviation for the build-up regime over land (see Fig. 4a).
- The main histogram characteristics of 'mixed' rain type are closer to the convective rain type than to stratiform, across both regimes and land-ocean areas.

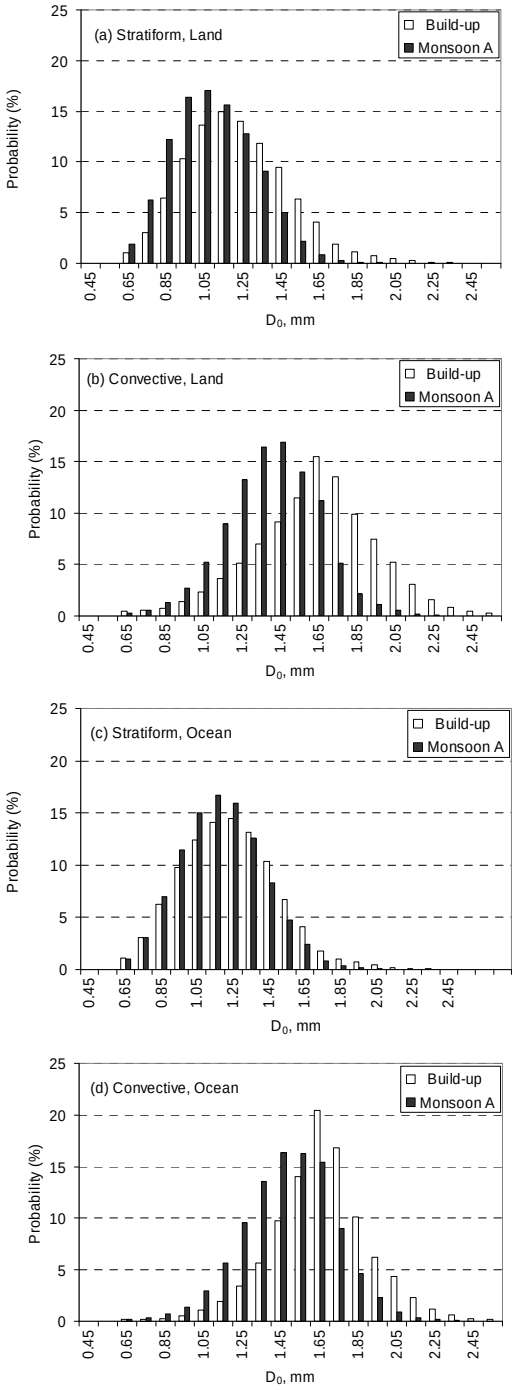

Fig, 7: Probability distributions of D_0 for (a) stratiform rain over land, (b) convective rain over land, (c) stratiform rain over ocean, and (d) convective rain over ocean. The bin centers have been slightly shifted for clarity.

- The main features of the histograms such as mean, width and skewness are very similar between land and ocean areas as one goes column wise in Table 1.

- The maximum value for mean D_0 (1.64 mm) and the broadest width (0.32 mm) occur for convective rain over land during the build-up regime.

Table 2 shows the same parameters for $\log_{10}(N_W)$ while Fig. 8 show the relative frequency histograms (in essence, the pdf). Again some points of note are:

- The main features of the histograms such as mean, width and skewness are very similar between land and ocean areas as one goes column wise in Table 2.

- The shapes are quite symmetric across both regimes, rain types and land-ocean areas.

- Since N_W generally is in inverse relation to D_0 (e.g., Testud et al. 2001), the mode of $\log_{10}(N_W)$ will shift oppositely to the shift in the mode of D_0, independent of regime, rain type or land-ocean areas.

- The main difference in the histograms is in Fig. 5b, i.e., between the build- up and Monsoon regimes for convective rain over land and less so over ocean (see Fig. 5d).

- Similar to above, the main difference in stratiform rain is between the build-up and Monsoon regimes over land (Fig. 5a) and less so over ocean (see Fig. 5c).

- Stratiform rain histograms show larger width compared to convective rain across both regimes and across land-ocean, except for the build-up regime over land.

- The main histogram characteristics of 'mixed' rain type are closer to the convective rain type than to stratiform, across both regimes and land-ocean areas.

Finally, in Fig. 9 we show the mean of $\log_{10}(N_W)$ versus the mean D_0 (along with respective $\pm 1\sigma$ error bars) for the stratiform and convective cases in blue and red, respectively. The two clusters are clearly clearly be seen. Also plotted in Fig. 6 are the range of values published in Table 2 of Ulbrich and Atlas (2007) for maritime convective storms and continental

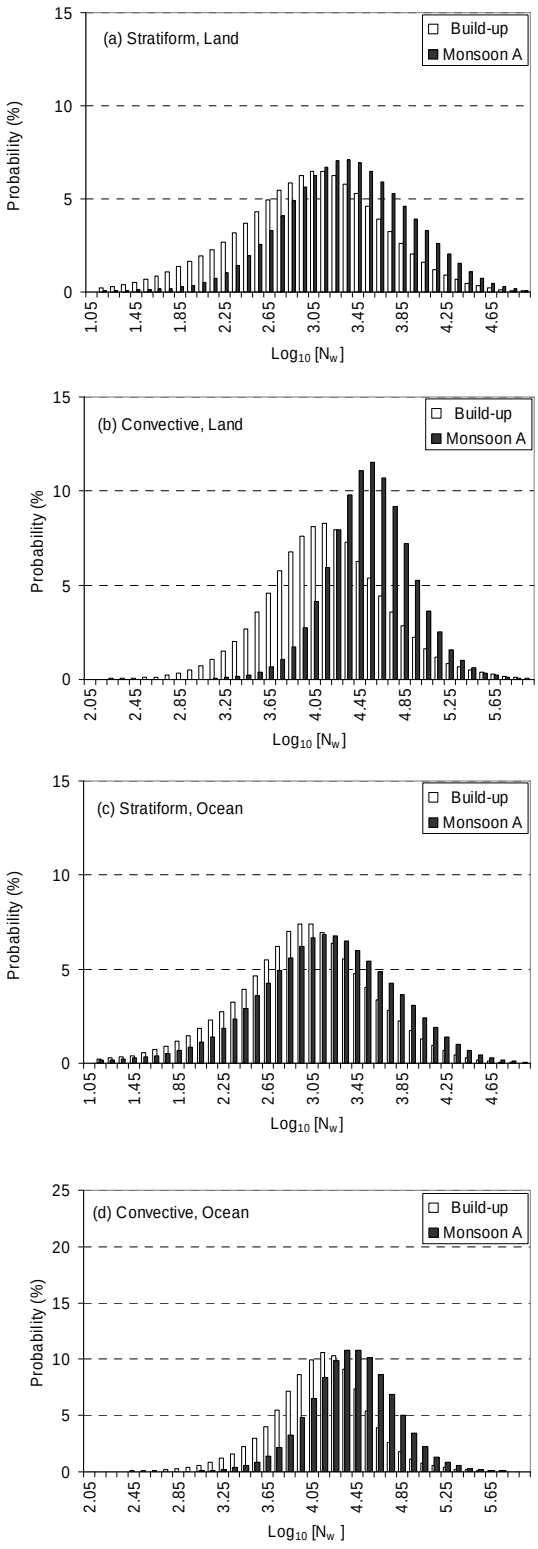

Fig. 8: PDFs of N_W corresponding to Fig. 4.

convective storms (in both cases as a brown line terminated with green-filled circles) with equilibrium or near-equilibrium DSDs. The maritime convective line falls well within our results for the convective events whilst the continental convective line falls well away from any of our results. Given that Darwin has a maritime climate, this agreement provides additional support for our retrievals and our classification scheme.

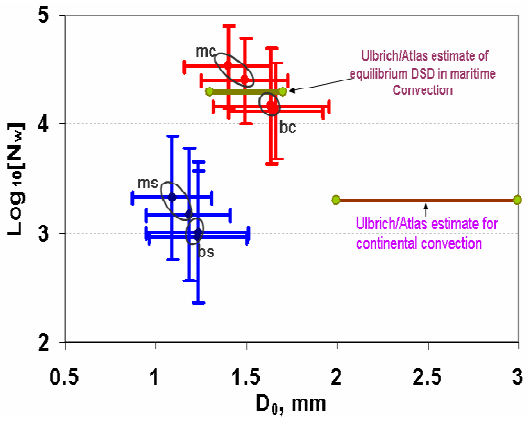

Fig. 9: Mean of $Log_{10}(N_W)$ versus mean of D_0 derived for convective (red) and stratiform rain types rain (blue), together with their respective standard deviations shown as error bars (±1σ). The Monsoon convective cases, build-up convective cases, Monsoon stratiform cases and build-up stratiform cases are circled and denoted by 'mc', 'bc', 'ms' and 'bs' respectively. Also plotted are the range of values published in Table 2 of Ulbrich and Atlas (2007) for maritime convective storms and continental convective storms (both as brown lines terminated with green-filled circles) for equilibrium or near-equilibrium DSDs.

5. CONCLUSIONS

The DSD-based indexing technique to automate the separation of stratiform and convective rain types has been tested methodically and in a robust manner using the CPOL radar data in Darwin. When compared with the previously published Z_h texture-based method, the indexing technique seems to perform equally well for stratiform rain and marginally better for convective rain. Our method has the advantage of being applied directly to PPI sweeps and more suitable for real-time application. It eliminates the need to generated CAPPIs, a process which might introduce interpolation errors.

The indexing method has been applied to the DSDs retrieved from all of the 1.1° elevation angle CPOL PPI sweeps taken during the TWP-ICE campaign. Two periods (regimes) were investigated, namely build-up and monsoon. The D_0 histograms show

TABLE 1: Mean, standard deviation, skewness of D_0 histograms, together with the percentage of cases and the total number of cases

LAND BUILD-UP	**Mean**	**Std. Dev.**	**Skewness**	**% of cases**	**No. of cases**
Stratiform	1.23	0.28	0.59	88.9	4936229
Convective	1.64	0.32	-0.16	8.4	466862
Mixed	1.46	0.32	0.07	2.6	146457
LAND MONSOON	**Mean**	**Std. Dev.**	**Skewness**	**% of cases**	**No. of cases**
Stratiform	1.09	0.22	0.39	89.6	5563841
Convective	1.40	0.24	-0.04	7.7	475606
Mixed	1.23	0.23	0.19	2.7	169378
OCEAN BUILD-UP	**Mean**	**Std. Dev.**	**Skewness**	**% of cases**	**No. of cases**
Stratiform	1.23	0.27	0.47	88.8	2541105
Convective	1.66	0.26	-0.01	8.7	248871
Mixed	1.49	0.28	0.20	2.5	71776
OCEAN MONSOON	**Mean**	**Std. Dev.**	**Skewness**	**% of cases**	**No. of cases**
Stratiform	1.18	0.23	0.32	87.7	2330923
Convective	1.49	0.24	-0.09	9.2	244589
Mixed	1.32	0.23	0.12	3.1	83524

TABLE 2: Mean, standard deviation, skewness of N_W histograms

LAND BUILD-UP	**Mean**	**Std. Dev.**	**Skewness**
Stratiform	3.01	0.65	-0.17
Convective	4.16	0.53	0.06
Mixed	3.91	0.54	-0.07
LAND MONSOON	**Mean**	**Std. Dev.**	**Skewness**
Stratiform	3.33	0.57	-0.15
Convective	4.53	.038	-0.06
Mixed	4.30	0.38	-0.19
OCEAN BUILD-UP	**Mean**	**Std. Dev.**	**Skewness**
Stratiform	2.97	0.60	-0.15
Convective	4.12	0.44	-0.20
Mixed	3.86	0.48	-0.21
OCEAN MONSOON	**Mean**	**Std. Dev.**	**Skewness**
Stratiform	3.17	0.61	-0.22
Convective	4.40	0.39	-0.08
Mixed	4.16	0.40	-0.12

noticeably larger values during build-up than the Monsoon period, as well as slightly lower N_W values. Comparison between land and ocean regions shows little difference except for the Monsoon case where slightly lower D_0 values are observed over land, together with slightly higher N_W values. Our N_W versus D_0 cluster of points for convective rain agree very well with previously published range of values for maritime convective DSDs. A significant implication is that the microphysical response to the differences in precipitation processes in tropical convective and stratiform clouds gives rise to a very clear and robust signature. This extends to convective clouds where warm rain processes are expected to dominate (Monsoon) or where ice processes are expected to dominate (build-up).

As additional material, in the Appendix, we present the conditioned PDFs of D_0 and $\log_{10}(N_W)$ (i.e. conditioned to dBZ intervals) for stratiform and convective rain, which are useful for improving rainfall retrieval algorithms for satellite based precipitation radar.

ACKNOWLEDGEMENTS

Partial support for this work is from the US Department of Energy (DOE) Atmospheric Radiation Measurement (ARM) program. One of the authors (MT) was supported by the US National Science Foundation via grant ATM-0603720. VNB acknowledges support from the NASA Precipitation Measurement Mission (PMM) program via grant NNX07AD47G. Michael Whimpey of the Centre for Australian Weather and Climate Research, Australia provided significant software support for this study.

REFERENCES

Atlas, D., C. W. Ulbrich, F.D. Marks, E. Amitai, and C. R. Williams, 1999: Systematic variation of drop size and radar-rainfall relations, *J. Geophys. Res.*, 104, no. D6, 6155 – 6169.

Atlas, D., C. W. Ulbrich, F.D. Marks, R.A. Black, E. Amitai, P.T. Willis and C.E. Samsury, 2000: Partitioning tropical oceanic convective and stratiform rains by draft strength. *J. Geophys. Res.*, 105, (D2), 2259–2267

Bringi, V.N. and V. Chandrasekar, 2001: Polarimetric Doppler Weather Radar: Principles and Applications, *Cambridge University Press*, 636 pp.

Bringi, V. N., V. Chandrasekar, J. Hubbert, E. Gorgucci, W. L. Randeu, and M. Schoenhuber, 2003: Raindrop Size Distribution in Different Climatic Regimes from Disdrometer and Dual-Polarized Radar Analysis, *J.Atmos. Sci.*, 60 (2), 354–365.

Bringi, V.N., C. R. Williams, M. Thurai and P.T May, 2009: Using dual-polarized radar and dual-frequency profiler for dsd characterization: a case study from Darwin, Australia, *J. Atmos. and Ocean. Tech.*, 2009 early online release, posted June 2009, DOI: 10.1175/2009JTECHA1258.1

Iguchi T., T. Kozu, R. Meneghini, J. Awaka, and K. Okamoto, 2000: Rain-profiling algorithm for the TRMM precipitation radar. *J. Appl. Meteor.*, 39, 2038–2052.

Joss, J. and A. Waldvogel, 1967: A raindrop spectrograph with automatic analysis. *Pure Appl. Geophys.*, 68, 240-246.

Keenan, T., K. Glasson, F. Cummings, T.S. Bird, R.J. Keeler and J. Lutz, 1998: The BMRC/NCAR C-band polarimetric (C-pol) radar system. *J. Atmos. Oceanic. Technol.*, 15, 871-886.

May, P.T., J. H. Mather, G. Vaughan, C. Jakob, G.M. McFarquhar, K.N. Bower, and G.G. Mace, 2008: The Tropical Warm Pool International Cloud Experiment. *Bulletin of the American Meteorological Society*, 89 (5), 629–645.

Steiner, M., R.A. Houze, Jr., and S.E. Yuter, 1995: Climatological characterization of three-dimensional storm structure from operational radar and rain gage data. *J. Appl. Meteor.*, 34, 1978-2007.

Testud, J., S. Oury, P. Amayenc and R.A. Black, 2001: The concept of “normalized” distributions to describe raindrop spectra: A tool for cloud physics and cloud remote sensing. *J. Appl. Meteor.*, 40, 1118-1140.

Tokay, A., and D.A. Short, 1996: Evidence from tropical raindrop spectra of the origin of rain from stratiform versus convective clouds. *J. Appl. Meteor.*, 35, 355-371.

Ulbrich, C.W., 1983: Natural variations in the analytical form of the raindrop size distribution. *J. Clim. Appl. Meteor.*, 22, 1764-1775.

Ulbrich, C.W., and D. Atlas, 2007: Microphysics of raindrop size spectra: Tropical continental and maritime storms. *J. Appl. Meteor. Climatol.*, 46, 1777-1791.

Williams, C. R., and K. S. Gage, 2009: Raindrop size distribution variability estimated using ensemble statistics, *Ann. Geophys.*, 27, 555-567, 2009.

Williams, C.R., W.L. Ecklund, and K.S. Gage, 1995: Classification of precipitating clouds in the Tropics using 915-MHz wind profilers. *J. Atmos. Oceanic. Technol.*, 12, 996-1012.

APPENDIX

CONDITIONED PDFS OF D_0 AND $LOG_{10}(N_W)$

Fig. A1 shows the conditioned PDFs of D_0 and $\log_{10}(N_W)$ for convective rain type with details being described in the caption. The most probable value for Z for this dataset was found to be in the interval 40-45 dBZ (third panel from left). In this interval the mode of D_0 is 1.65 mm for build-up and 1.3 mm for the Monsoon regime; correspondingly, the mode of N_W is 10,000 mm^{-1} m^{-3} and 30,000 (factors of 1.25 and 3.75 larger than the Marshall-Palmer value of 8000). Such PDFs are valuable for example, in determining whether or not the PR-2A25 α-adjustment procedure (Iguchi et al 2000) can adjust the DSD parameters for convective rain in both regimes consistent with the PDFs shown in Fig. A1.

Fig. A2 shows similar PDFs for stratiform rain over land, again contrasting build-up versus Monsoon regimes. The most probable value for Z for this stratiform rain dataset was found to be in the interval 20-25 dBZ (second panel from left). In this interval the mode of D_0 is near 1.25 mm for both build-up and Monsoon regimes; correspondingly, the mode of N_W is near 1800 mm^{-1} m^{-3} (factor of 4.5 less than the Marshall-Palmer value of 8000).

A further point of interest is that in the dBZ intervals of 30 – 35 dBZ, and 35 – 40 dBZ, stratiform rain shows D_0 with a higher mode than convective rain, both for the build-up and monsoon regimes.

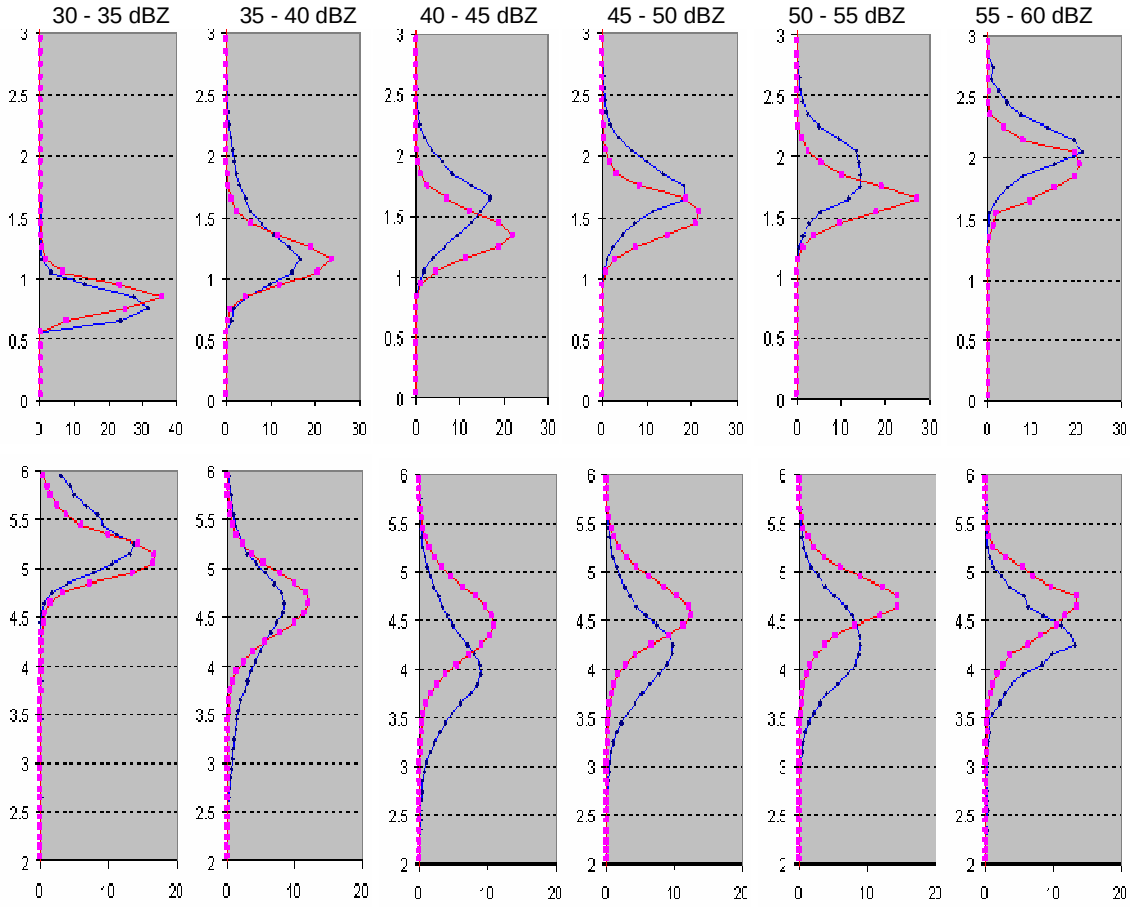

Fig. A1: PDFs of D_0 (top 6 panels) for convective rain over land. Blue curves are for build-up regime whilst pink curves are for Monsoon. The abscissa is the relative frequency (%) while the ordinate is D_0 in mm. The PDFs are conditioned on the Z interval with leftmost panel being the interval 30-35 dBZ and stepping up by 5 dB to the rightmost panel interval being 55-60 dBZ. The bottom 6 panels are the conditioned PDFs of $\log_{10}(N_W)$ with the ordinate being the value of $\log_{10}(N_W)$ and the abscissa being the relative frequency (%).

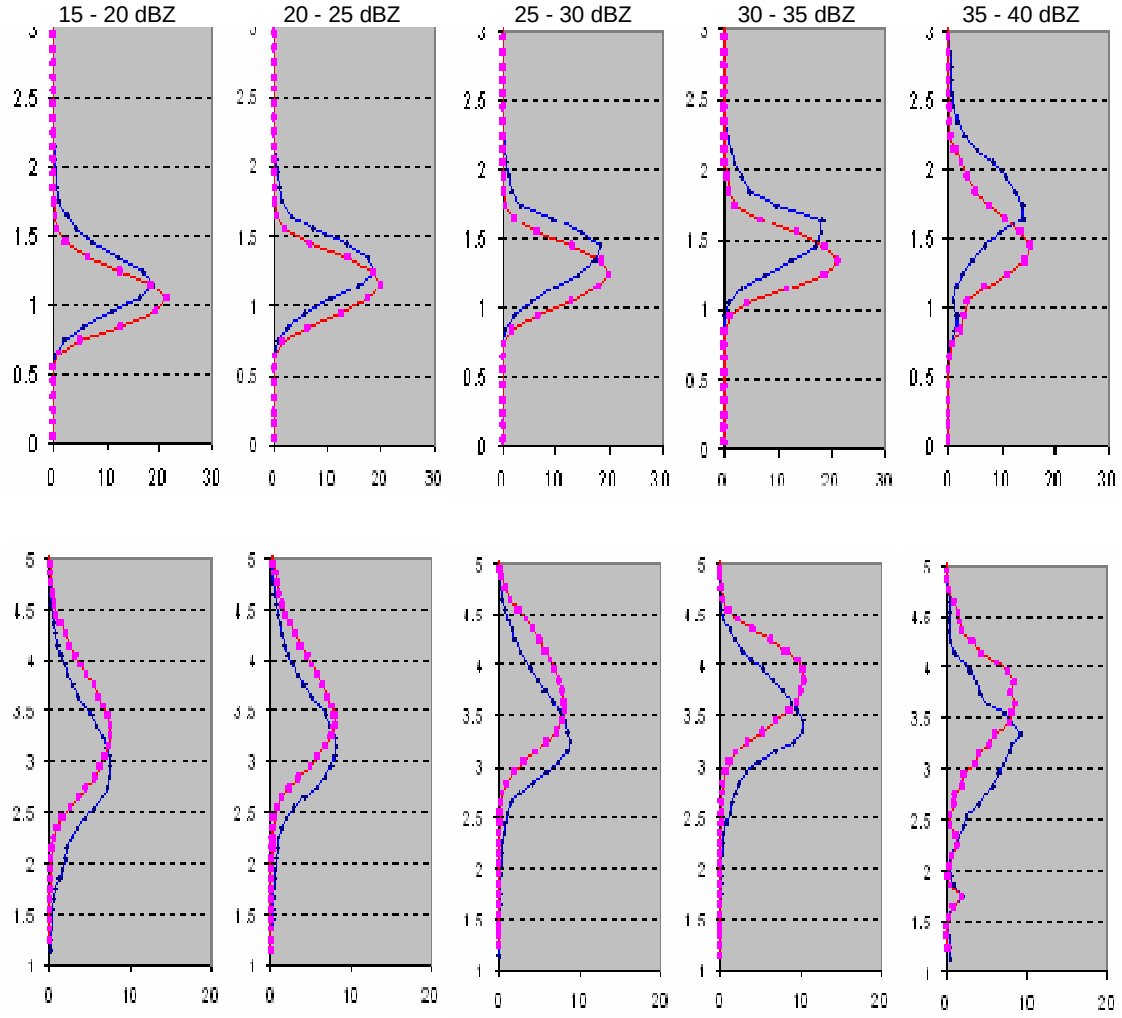

Fig. A2: As in Fig. A1 except for stratiform rain. The PDFs are conditioned by the Z interval being 15-20 dBZ for the leftmost panel and stepping up by 5 dB to the rightmost panel interval being 35-40 dBZ.